Three-Dimensional Stagnation-Point Flow and Heat Transfer of a Dusty Fluid Toward a Stretching Sheet

M. R. Mohaghegh
Faculty of Engineering,
Ferdowsi University of Mashhad,
P.O. Box No. 91775-1111,
Mashhad 9177948974, Iran

Asghar B. Rahimi[1]
Professor
Faculty of Engineering,
Ferdowsi University of Mashhad,
P.O. Box No. 91775-1111,
Mashhad 9177948974, Iran
e-mail: rahimiab@yahoo.com

The steady three-dimensional stagnation-point flow and heat transfer of a dusty fluid toward a stretching sheet is investigated by using similarity solution approach. The free-stream along z-direction impinges on the stretching sheet to produce a flow with different velocity components. The governing equations are transformed into ordinary differential equations by introducing appropriate similarity variables and an exact solution is obtained. The nonlinear ordinary differential equations are solved numerically using Runge–Kutta fourth-order method. The effects of the physical parameters like velocity ratio, fluid and thermal particle interaction parameter, ratio of freestream velocity parameter to stretching sheet velocity parameter, Prandtl number, and Eckert number on the flow field and heat transfer characteristics are obtained, illustrated graphically, and discussed. Also, a comparison of the obtained numerical results is made with two-dimensional cases existing in the literature and good agreement is approved. Moreover, it is found that the heat transfer coefficient and shear stress on the surface for axisymmetric case are larger than nonaxisymmetric case. Also, for stationary flat plat case, a similarity solution is presented and a comparison of the obtained results is made with previously published results and full agreement is reported. [DOI: 10.1115/1.4033614]

Keywords: three-dimensional stagnation-point flow, exact solution, similarity variables, dusty fluid, fluid-particle interaction parameter, stretching sheet

1 Introduction

Analysis of boundary layer flow and heat transfer over a stretching sheet has been considered significantly in recent years due to its applications. This problem has many engineering applications in industrial processes, such as polymer industry involving cooling of a molten liquid, rolling and manufacturing of sheets and fibers, paper production, drawing of plastic film, and so on. Particularly, when the flow is a mixture of solid–fluid (dusty flow), its analysis has importance and application in combustion, petroleum transport, corrosive particles in engine oil flow, wastewater treatment, etc.

One of the pioneering studies in this field is by Sakiadis [1] who studied the boundary layer flow behavior over a stretched sheet with a constant velocity. Crane [2] investigated the analytical study of boundary layer flow over a linearly stretching sheet and presented an exact solution for the flow field.

Many exact solutions for Navier–Stokes and energy equations regarding the problem of stagnation-point flow and heat transfer in the vicinity of a plane have been found. Hiemenz [3] and Homman [4] did the first study in this field for two-dimensional and axisymmetric cases, respectively. Chiam [5] studied steady two-dimensional stagnation-point flow of an incompressible viscous fluid toward a stretching sheet. Ishak et al. [6,7] studied the flow and heat transfer characteristics over a stretching sheet and stagnation-point flow toward a stretching sheet in the presence of a uniform magnetic field. Tzirtzilakis and Kafoussias [8] investigated the three-dimensional laminar and steady boundary layer flow of an electrically nonconducting and incompressible magnetic fluid, with low Curie temperature and moderate saturation magnetization, over an elastic stretching sheet. Abbassi and Rahimi [9,10] presented an exact solution of the Navier–Stokes and energy equations using similarity solution approach for problem of three-dimensional stagnation-point flow and heat transfer on a flat plate with and without transpiration. Also, Abbassi et al. [11] analyzed the unsteady case of this problem. Further, Abbassi and Rahimi [12] studied a two-dimensional unsteady stagnation-point flow and heat transfer impinging on an accelerated flat plate. Kuznetsov and Nield [13,14] solved problem of natural convective boundary-layer flow of a nanofluid past a vertical plate analytically by similarity solution. Mustafa et al. [15] studied stagnation-point flow of a nanofluid toward a stretching sheet. Also, Makinde et al. [16] investigated buoyancy effects on magneto-hydrodynamic (MHD) stagnation-point flow and heat transfer of a nanofluid past a convectively heated stretching/shrinking sheet. Mahapatra et al. [17] presented a similarity solution for steady two-dimensional MHD stagnation-point flow and heat transfer of an incompressible viscous fluid over a stretching/shrinking sheet in the presence of velocity and thermal slips. Sinha and Misra [18] studied MHD stagnation-point flow of an incompressible viscous electrically conducting fluid over a stretching sheet.

In all the above cited papers, the fluid considered was viscous, incompressible, and free from impurities. But, in nature, the fluid in pure form is rarely available. Air and water contains impurities like dust particles and foreign bodies. In recent years, researchers have turned to studying dusty fluid. Therefore, the studying two-phase flows in which solid spherical particles are distributed in a clean fluid are of interest in practical applications like petroleum industry.

Fundamental studies in dynamics of dusty fluid, its behavior, and boundary layer modeling have been considered in literature including Refs. [19–22]. Vajravelu and Nayfeh [23] analyzed the hydromagnetic flow of a dusty fluid over a stretching sheet including the effects of suction. Gireesha et al. [24] investigated the effect of viscous dissipation and heat source on flow and heat transfer of dusty fluid over an unsteady stretching sheet. Further, Gireesha et al. [25] studied steady boundary layer flow and heat transfer of a dusty fluid flow over a stretching sheet with

[1]Corresponding author.

Contributed by the Heat Transfer Division of ASME for publication in the Journal of Heat Transfer. Manuscript received July 27, 2015; final manuscript received May 11, 2016; published online June 14, 2016. Assoc. Editor: Andrey Kuznetsov.

nonuniform heat source/sink. Ramesh and Gireesha [26] analyzed radiation effect on a steady two-dimensional boundary layer flow of a dusty fluid over a stretching sheet. Further, recent works [23–29] have been done in the area of dusty flow over a stretching sheet or plate under different effects and conditions.

In all the above cited papers with a dusty fluid flow, the problem is modeled and analyzed just for the two-dimensional cases. To our knowledge, no attempts have been made to analyze three-dimensional stagnation-point flow of a dusty fluid toward a stretching sheet.

The objective of the present study is to investigate the three-dimensional stagnation-point flow of a dusty fluid toward a stretching sheet by solving Navier–Stokes and energy equations for both fluid and particle flows. Appropriate similarity variables for governing equations are derived in this problem. The obtained ordinary differential equations are solved numerically by using Runge–Kutta fourth-order method. Velocity and temperature profiles are presented for different values of velocity ratio, fluid and thermal particle interaction parameter, ratio of freestream velocity parameter to stretching sheet velocity parameter, Prandtl number, and Eckert number for both of the fluid and dust phases. Also, a comparison of the obtained numerical results for two-dimensional problem is made with those of Refs. [28,30] and excellent agreement is reported. Our main goal here is to present a model for combustion in a stagnation-point flow problem where the fluid phase changes into vaporized bubbles upon impact on a heated substrate and thereafter could go through the process of combustion if ignition takes place.

2 Problem Formulation

Consider a steady, three-dimensional, incompressible, laminar boundary layer flow and heat transfer of an incompressible viscous dusty fluid in the neighborhood of stagnation-point flow over a stretching surface. The problem is formulated in Cartesian coordinates (x, y, z) with corresponding velocity components (u, v, w). The stretching surface is placed in the plane $z = 0$, with the flow being confined to $z > 0$ as the schematic geometry shown in Fig. 1.

The stretching surface velocities in the x- and y-directions, respectively, are given by

$$u_w = c\lambda x, \quad v_w = cy \tag{1}$$

where $c > 0$ is the stretching rate and λ is the coefficient which indicates the difference between the sheet velocity components in x and y directions. The dust particles are treated as spheres with uniform size and their number density are taken as a constant throughout the flow.

The three-dimensional boundary layer equations for clean fluid and dusty particles with usual notation are Refs. [16,19]:

continuity

$$\frac{\partial u}{\partial x} + \frac{\partial v}{\partial y} + \frac{\partial w}{\partial z} = 0 \tag{2}$$

$$\frac{\partial}{\partial x}(\rho_p u_p) + \frac{\partial}{\partial y}(\rho_p v_p) + \frac{\partial}{\partial z}(\rho_p w_p) = 0 \tag{3}$$

momentum

$$\rho\left(u\frac{\partial u}{\partial x} + v\frac{\partial u}{\partial y} + w\frac{\partial u}{\partial z}\right) = -\frac{\partial p}{\partial x} + \mu\left(\frac{\partial^2 u}{\partial x^2} + \frac{\partial^2 u}{\partial y^2} + \frac{\partial^2 u}{\partial z^2}\right) + F_{px} \tag{4}$$

$$\rho\left(u\frac{\partial v}{\partial x} + v\frac{\partial v}{\partial y} + w\frac{\partial v}{\partial z}\right) = -\frac{\partial p}{\partial y} + \mu\left(\frac{\partial^2 v}{\partial x^2} + \frac{\partial^2 v}{\partial y^2} + \frac{\partial^2 v}{\partial z^2}\right) + F_{py} \tag{5}$$

$$\rho\left(u\frac{\partial w}{\partial x} + v\frac{\partial w}{\partial y} + w\frac{\partial w}{\partial z}\right) = -\frac{\partial p}{\partial y} + \mu\left(\frac{\partial^2 w}{\partial x^2} + \frac{\partial^2 w}{\partial y^2} + \frac{\partial^2 w}{\partial z^2}\right) + F_{pz} \tag{6}$$

$$\rho_p\left(u_p\frac{\partial u_p}{\partial x} + v_p\frac{\partial u_p}{\partial y} + w_p\frac{\partial u_p}{\partial z}\right) = -F_{px} \tag{7}$$

$$\rho_p\left(v_p\frac{\partial v_p}{\partial x} + v_p\frac{\partial v_p}{\partial y} + w_p\frac{\partial v_p}{\partial z}\right) = -F_{py} \tag{8}$$

$$\rho_p\left(u_p\frac{\partial w_p}{\partial x} + v_p\frac{\partial w_p}{\partial y} + w_p\frac{\partial w_p}{\partial z}\right) = -F_{pz} \tag{9}$$

energy

$$\rho c_p\left(u\frac{\partial T}{\partial x} + v\frac{\partial T}{\partial y} + w\frac{\partial T}{\partial z}\right) = k\frac{\partial^2 T}{\partial y^2} + Q_p + (u_p - u)F_{p_x} + (v_p - v)F_{p_y} \tag{10}$$

$$\rho_p c_m\left(u_p\frac{\partial T_p}{\partial x} + v_p\frac{\partial T_p}{\partial y} + w_p\frac{\partial T_p}{\partial z}\right) = -Q_p \tag{11}$$

where (u, v, w) and (u_p, v_p, w_p) are the velocity components of the fluid and dust phases along the x, y, and z directions, respectively. p, ρ, ρ_p, and μ are fluid pressure, density of the fluid, density of the dust phase, and viscosity of the fluid, respectively. Also, in energy equations, T and T_p are the temperature of the fluid and temperature of the dust phase, and k is the thermal conductivity of the fluid.

The terms F_{p_i}, Q_p, and $(V_{p_i} - V_i)F_{p_i}$, represent, respectively, the particles force on fluid along i direction (the drag force due to the interaction between the fluid and dust phases), the heat transferred from particle phase to fluid phase, and the dissipation work due to particles moving relative to the fluid per unit volume and are expressed as follows:

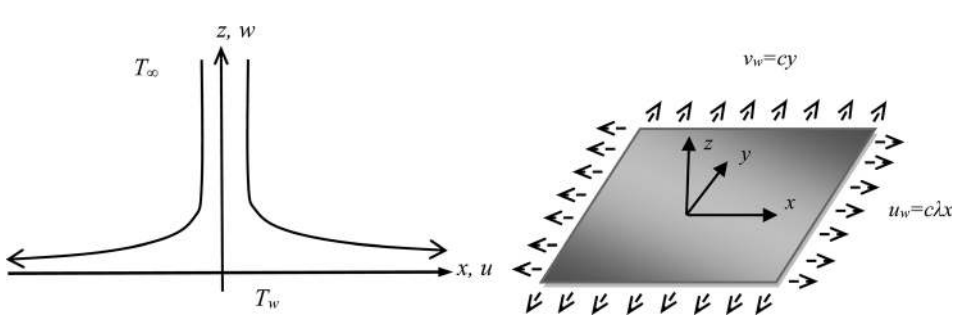

Fig. 1 Schematic geometry of the flow configuration

$$F_{p_i} = N.6\pi\sigma\mu(V_{p_i} - V_i) = \rho_p \frac{V_{p_i} - V_i}{\tau_v} \tag{12}$$

$$Q_p = N.4\pi\sigma k_p(T_p - T) = \rho_p c_p \frac{T_p - T}{\tau_T} \tag{13}$$

where V_i and V_{p_i} are velocity vector of the fluid and dusty phases, respectively, σ is the particle radius, k_p is thermal conductivity of the particle, N is number density of the dust phase, τ_v is the relaxation time of the dust phase that expresses the time required by the particle cloud (dust) to reduce its velocity relative to the fluid, and τ_T is the thermal equilibrium time that expresses the time required by the particle cloud to reduce its temperature relative to the fluid.

The velocity components of the classical potential flow solution are as follows [9,10]:

$$U = a\lambda x \tag{14}$$

$$V = ay \tag{15}$$

$$W = -a(\lambda + 1)z \tag{16}$$

where $0 < \lambda \leq 1$ is presented as the ratio of the velocity components in x and y directions which indicates the difference between the velocity components in x and y directions and $a > 0$ is a constant. For $\lambda = 1$, freestream velocity components in x and y directions are the same, and also the sheet velocity components are the same in these directions, too. So, the problem will be converted into an axisymmetric problem with no difference between the flow characteristics in x and y directions.

Employing the Bernoulli's equation in the potential region, the following relations between the freestream velocity $U(x)$ and $V(y)$ and the pressure gradients in x and y directions are specified, respectively

$$-\frac{1}{\rho}\frac{\partial p}{\partial x} = U\frac{dU}{dx} \tag{17a}$$

$$-\frac{1}{\rho}\frac{\partial p}{\partial y} = V\frac{dV}{dy} \tag{17b}$$

Using Eqs. (12)–(17) into Eqs. (4), (5), and (7)–(11), one can obtain

$$u\frac{\partial u}{\partial x} + v\frac{\partial u}{\partial y} + w\frac{\partial u}{\partial z} = U\frac{dU}{dx} + \upsilon\left(\frac{\partial^2 u}{\partial x^2} + \frac{\partial^2 u}{\partial y^2} + \frac{\partial^2 u}{\partial z^2}\right) + \frac{\rho_p}{\rho\tau_v}(u_p - u) \tag{18}$$

$$u\frac{\partial v}{\partial x} + v\frac{\partial v}{\partial y} + w\frac{\partial v}{\partial z} = V\frac{dV}{dy} + \upsilon\left(\frac{\partial^2 v}{\partial x^2} + \frac{\partial^2 v}{\partial y^2} + \frac{\partial^2 v}{\partial z^2}\right) + \frac{\rho_p}{\rho\tau_v}(v_p - v) \tag{19}$$

$$u_p\frac{\partial u_p}{\partial x} + v_p\frac{\partial u_p}{\partial y} + w_p\frac{\partial u_p}{\partial z} = \frac{1}{\tau_v}(u - u_p) \tag{20}$$

$$u_p\frac{\partial v_p}{\partial x} + v_p\frac{\partial v_p}{\partial y} + w_p\frac{\partial v_p}{\partial z} = \frac{1}{\tau_v}(v - v_p) \tag{21}$$

$$u_p\frac{\partial w_p}{\partial x} + v_p\frac{\partial w_p}{\partial y} + w_p\frac{\partial w_p}{\partial z} = \frac{1}{\tau_v}(w - w_p) \tag{22}$$

$$u\frac{\partial T}{\partial x} + v\frac{\partial T}{\partial y} + w\frac{\partial T}{\partial z} = \alpha\frac{\partial^2 T}{\partial y^2} + \frac{\rho_p}{\rho}\frac{T_p - T}{\tau_T} + \frac{\rho_p}{\rho c_p}\frac{1}{\tau_v}\left[(u_p - u)^2 + (v_p - v)^2\right] \tag{23}$$

$$u_p\frac{\partial T_p}{\partial x} + v_p\frac{\partial T_p}{\partial y} + w_p\frac{\partial T_p}{\partial z} = \frac{c_p}{c_m}\frac{T - T_p}{\tau_T} \tag{24}$$

where υ, α, c_p, and c_m are kinematic viscosity, thermal diffusivity, the specific heat of fluid, and dust phase, respectively. It is assumed that $c_p = c_m$ throughout this study.

3 Similarity Solution

3.1 Fluid Flow Solution. To convert partial differential equations into a set of ordinary differential equations, the following dimensionless similarity variables are introduced:

$$\begin{aligned} &u = c\lambda x f'(\eta), \quad v = cy\left[f'(\eta) + g'(\eta)\right], \\ &w = -\sqrt{c\nu}\left[g(\eta) + (\lambda + 1)f(\eta)\right], \quad \eta = \sqrt{\frac{c}{\nu}}z \\ &u_p = c\lambda x F(\eta), \quad v_p = cy\left[F(\eta) + G(\eta)\right], \\ &\mathrm{w}_p = \sqrt{c\nu}\left[G(\eta) + (\lambda + 1)K(\eta)\right], \quad \rho_r = \frac{\rho_p}{\rho} = H(\eta) \end{aligned} \tag{25}$$

Substituting transformations (25) into momentum Eqs. (18)–(22) and continuity Eq. (3) yields the following nonlinear ordinary differential equations:

$$f''' + [g + (\lambda + 1)f]f'' + \lambda(\gamma^2 - f'^2) + \beta(F - f')H = 0 \tag{26}$$

$$g''' + [g + (\lambda + 1)f]g'' - (g' + 2f')g' - (1 - \lambda)(f'^2 - \gamma^2) + \beta(G - g')H = 0 \tag{27}$$

$$[G + (\lambda + 1)K]F' + \lambda F^2 + \beta(F - f') = 0 \tag{28}$$

$$[G + (\lambda + 1)K]G' - \lambda F^2 + (G + F)^2 + \beta(G - g') = 0 \tag{29}$$

$$[G + (\lambda + 1)K][(\lambda + 1)K' + G'] + \beta[G + g + (\lambda + 1)(K + f)] = 0 \tag{30}$$

$$[G + (\lambda + 1)K]H' + [(\lambda + 1)(F + K') + G + G']H = 0 \tag{31}$$

where the prime sign denotes differentiation with respect to η, and $\beta = 1/c\tau_\nu$ is the fluid-particle interaction parameter, $\gamma = a/c$ is the ratio of the freestream velocity parameter to the stretching sheet parameter and $H = \rho_r = \rho_p/\rho$ is the relative density. The boundary conditions for the above equations are

$$\eta = 0 : \begin{cases} u = u_w, \ v = v_w, \ w = 0 \\ f' = 1, f = 0, g = g' = 0 \end{cases} \tag{32}$$

$$\eta \to \infty : \begin{cases} u_p = u = U, \ v_p = v = V, \ w_p = W, \rho_p = \rho\omega \\ f' = F = \lambda, g' = G = 0, K = -f - \dfrac{g}{(\lambda + 1)}, H = \omega \end{cases} \tag{33}$$

where ω is the density ratio and is taken as the value of 0.2 in this study.

3.2 Heat Transfer Solution. To transform the energy equation into a nondimensional form, dimensionless temperature profiles for the clean fluid and the dusty fluid are introduced as follows:

$$\theta(\eta) = \frac{T - T_\infty}{T_w - T_\infty}, \quad \theta_p(\eta) = \frac{T_p - T_\infty}{T_w - T_\infty} \tag{34}$$

where T_w and T_∞ denote the temperature at wall and the infinity, respectively, which are assumed to be a constant. By using

Eqs. (25) and (34) into Eqs. (23) and (24), the energy equations are obtained as

$$\theta'' + \Pr[g + (\lambda+1)f]\theta' + \Pr\beta_T[\theta_p - \theta]H + \Pr\beta[\mathrm{Ec}_x(F - f')^2 + \mathrm{Ec}_y(F - f' + G - g')^2]H = 0 \quad (35)$$

$$[G + (\lambda+1)K]\theta_p' + \frac{c_p}{c_m}\beta_T[\theta_p - \theta] = 0 \quad (36)$$

where $\Pr = \mu c_p/k$ is the Prandtl number, $\mathrm{Ec}_x = (cx\lambda)^2/c_p\Delta T$ and $\mathrm{Ec}_y = (cy)^2/c_p\Delta T$ ($\Delta T = T_w - T_\infty > 0$) are the Eckert numbers, and $\beta_T = 1/c\tau_T$ is the fluid–particle interaction parameter for temperature (thermal fluid–particle interaction parameter). The boundary conditions for Eqs. (35) and (36) are as

$$\eta = 0: \; T = T_w \rightarrow \theta = 1 \quad (37)$$

$$\eta \rightarrow 0: T = T_p = T_\infty \rightarrow \theta_p = \theta = 0 \quad (38)$$

The special case of a stationary plate is considered next in Sec. 4.

Table 1 Comparison of the values of velocity gradient in the *x* direction $f''(0)$ for the different values of γ when β=0

γ	Ref. [26]	Ref. [24]	Present study (2D)	Present study (3D axi.; $\lambda = 1$)
0.1	−0.9737	−0.9696	−0.9697	−1.1246
0.2	−0.9215	−0.9181	−0.9182	−1.0556
0.5	−0.6676	−0.6672	−0.6672	−0.7534
2.0	2.0174	2.0175	2.0175	2.2071
3.0	4.7290	4.7292	4.7293	5.1366

Table 2 The shear stress coefficients in the *x* direction $\lambda f''(0)$, the *y* direction $f''(0)+g''(0)$, and heat transfer coefficient on the wall $\theta'(0)$ when β=0, β_T=0, Ec_x=0, and Ec_y=0

γ	Λ	$\lambda f''(0)$	$f''(0) + g''(0)$	$\theta'(0)$
0.2	0.25	−0.1713	−0.9563	−0.5847
	0.5	−0.4141	−0.9912	−0.6438
	0.75	−0.7117	−1.0241	−0.6965
	1	−1.0556	−1.0556	−0.7447
2	0.25	0.3444	2.0633	−0.9303
	0.5	0.8481	2.1106	−1.0147
	0.75	1.4755	2.1587	−1.0943
	1	2.2071	2.2071	−1.1694

4 Stationary Flat Plate

Here, the special case of the three-dimensional stagnation-point flow of a dusty fluid toward a stationary flat plate is investigated. If in the stretching sheet problem, the sheet velocity tends to zero ($c \rightarrow 0$), then the similarity parameter $\eta \rightarrow 0$ and the parameter $\gamma = a/c$ are meaningless. Therefore, for a stationary flat plate ($c = 0$), we need to define a new dimensionless parameter. For this problem, the similarity variables are defined as the following:

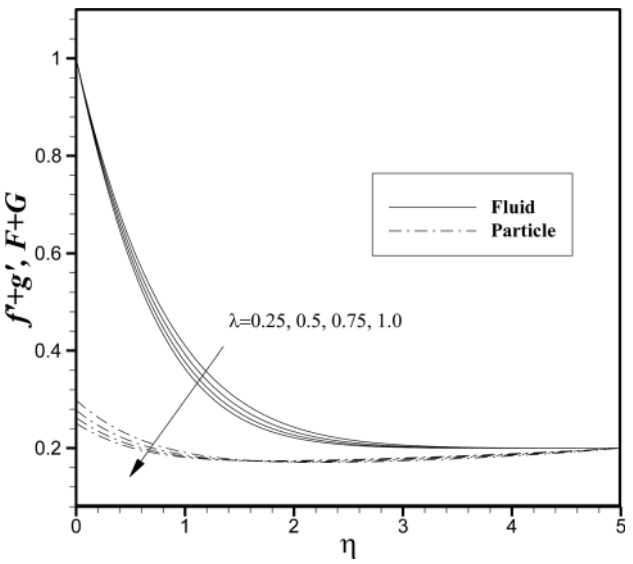

Fig. 3 Dimensionless profiles of *v*, v_p velocity components for different values of λ when $\gamma = 0.2$ and $\beta = 0.5$

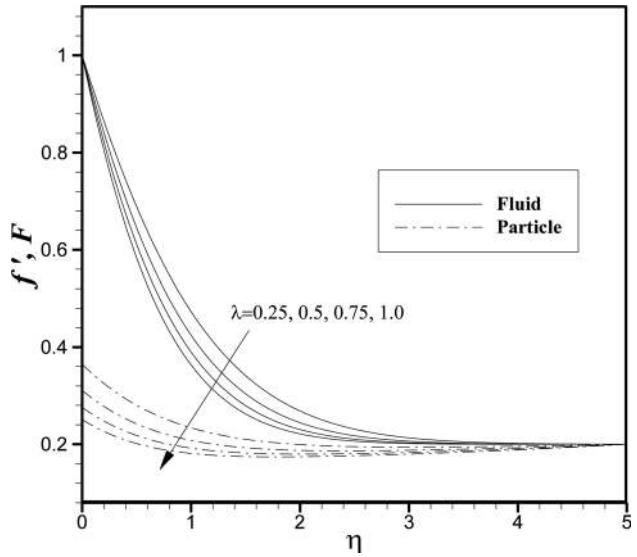

Fig. 2 Dimensionless profiles of *u*, u_p velocity components for different values of λ when $\gamma = 0.2$ and $\beta = 0.5$

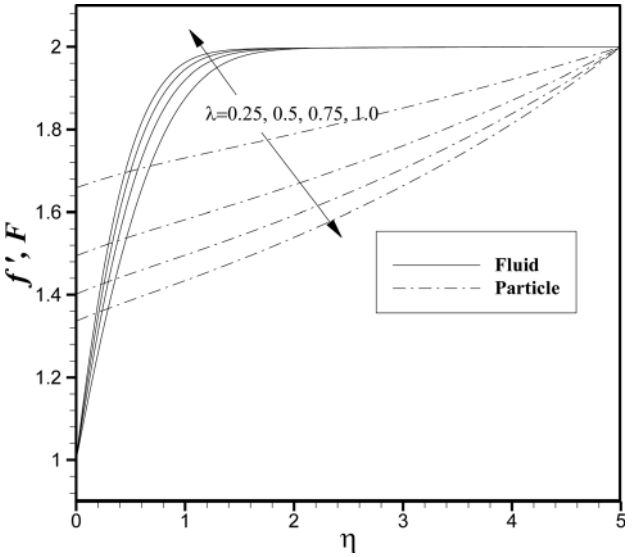

Fig. 4 Dimensionless profiles of *u*, u_p velocity components for different values of λ when $\gamma = 2.0$ and $\beta = 0.5$

$$u = a\lambda x f'(\eta), \quad v = ay\left[f'(\eta) + g'(\eta)\right],$$
$$w = -\sqrt{a\nu}\left[g(\eta) + (\lambda+1)f(\eta)\right], \quad \eta = \sqrt{\frac{a}{\nu}}z$$
$$u_p = a\lambda x F(\eta), \quad v_p = ay\left[F(\eta) + G(\eta)\right], \tag{39}$$
$$w_p = \sqrt{a\nu}\left[G(\eta) + (\lambda+1)K(\eta)\right], \quad \rho_r = \frac{\rho_p}{\rho} = H(\eta)$$

Substituting these transformations into momentum Eqs. (18)–(22) and continuity Eq. (3) yields the following nonlinear ordinary differential equations:

$$f''' + [g + (\lambda+1)f]f'' + \lambda(1 - f'^2) + \beta'(F - f')H = 0 \tag{40}$$

$$g''' + [g + (\lambda+1)f]g'' - (g' + 2f')g' - (1-\lambda)(f'^2 - 1) + \beta'(G - g')H = 0 \tag{41}$$

$$[G + (\lambda+1)K]F' + \lambda F^2 + \beta'(F - f') = 0 \tag{42}$$

$$[G + (\lambda+1)K]G' - \lambda F^2 + (G+F)^2 + \beta'(G - g') = 0 \tag{43}$$

$$[G + (\lambda+1)K][(\lambda+1)K' + G'] + \beta'[G + g + (\lambda+1)(K+f)] = 0 \tag{44}$$

$$[G + (\lambda+1)K]H' + [(\lambda+1)(F+K') + G + G']H = 0 \tag{45}$$

where $\beta' = 1/a\tau_\nu$ is the new fluid–particle interaction parameter. The boundary conditions for the above equations are

$$\eta = 0: \begin{cases} u = 0, \ v = 0, \ w = 0 \\ f' = 0, f = 0, g = g' = 0 \end{cases} \tag{46}$$

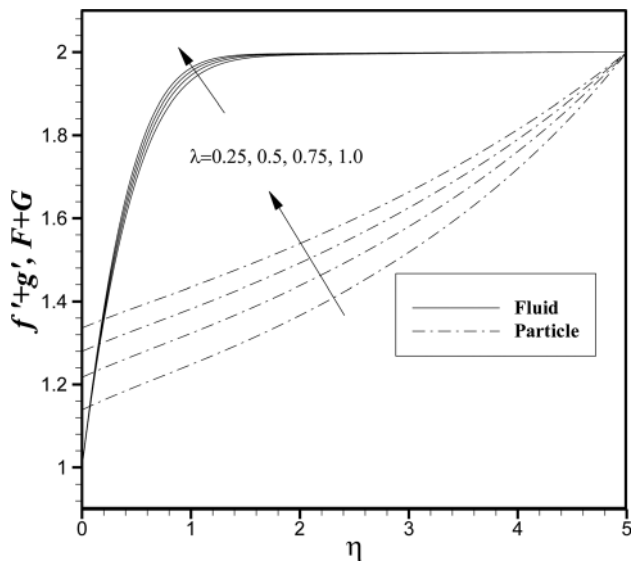

Fig. 5 Dimensionless profiles of v, v_p velocity components for different values of λ when $\gamma = 2.0$ and $\beta = 0.5$

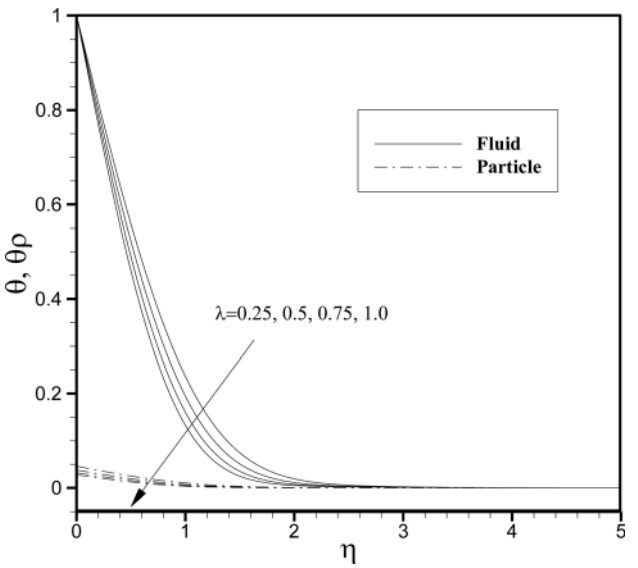

Fig. 7 Dimensionless temperature profiles for different values of λ when $\beta = 0.5$, $\beta_T = 0.5$, Pr = 0.72, $Ec_x = Ec_y = 1.0$, and $\gamma = 2.0$

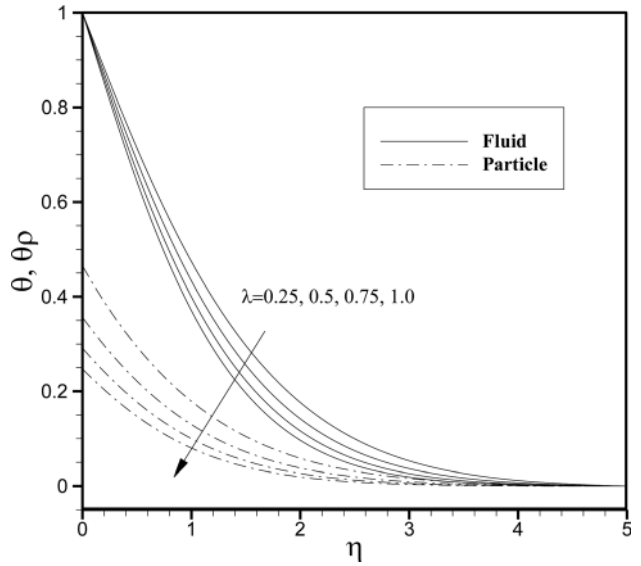

Fig. 6 Dimensionless temperature profiles for different values of λ when $\beta = 0.5$, $\beta_T = 0.5$, Pr = 0.72, $Ec_x = Ec_y = 1.0$, and $\gamma = 0.2$

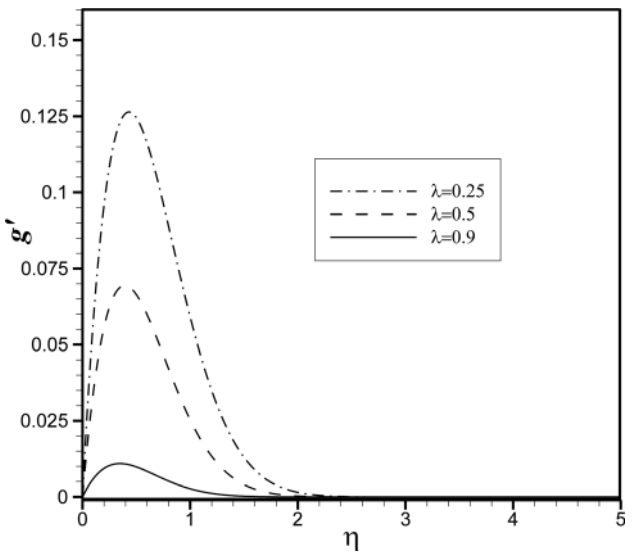

Fig. 8 Effect of the velocity ratio λ on g' profiles when $\gamma = 2.0$ and $\beta = 0.5$

$$\eta \to \infty : \begin{cases} u_p = u = U,\ v_p = v = V,\ w_p = W, \rho_p = \rho\omega \\ f' = F = 1, g' = G = 0, K = -f - \dfrac{g}{(\lambda+1)}, H = \omega \end{cases} \tag{47}$$

Similarly, by using the definition of the dimensionless temperature profiles from Eqs. (34) and (39), into Eqs. (23) and (24), the energy equations are obtained as

$$\theta'' + \Pr[g + (\lambda+1)f]\theta' + \Pr\beta'_T[\theta_p - \theta]H + \Pr\beta'[\mathrm{Ec}_x(F - f')^2 + \mathrm{Ec}_y(F - f' + G - g')^2]H = 0 \tag{48}$$

$$[G + (\lambda+1)K]\theta'_p + \frac{c_p}{c_m}\beta'_T[\theta_p - \theta] = 0 \tag{49}$$

where $\beta'_T = 1/a\tau_T$ is the new fluid–particle interaction parameter for the temperature. The boundary conditions for the above equations are as

$$\eta = 0 :\ T = T_w \to \theta = 1 \tag{50}$$

$$\eta \to 0 : T = T_p = T_\infty \to \theta_p = \theta = 0 \tag{51}$$

Some numerical results are presented in Sec. 5.

5 Results and Discussion

Equations (26)–(31) and Eqs. (35) and (36) with the boundary conditions (32) and (33) and (37) and (38), respectively, are two set of coupled highly nonlinear ordinary differential equations. To solve these equations, we applied the fourth-order Runge–Kutta numerical scheme with a shooting method for Eqs. (26), (27), and (35) and iterated the solution process till satisfying the initial boundary conditions. The fourth-order Runge–Kutta numerical method is a convenient and efficient method to solve a boundary value problem.

In this section, the solution of the self-similar Eqs. (26)–(31), (35), and (36) for different values of the fluid velocity ratio λ, the

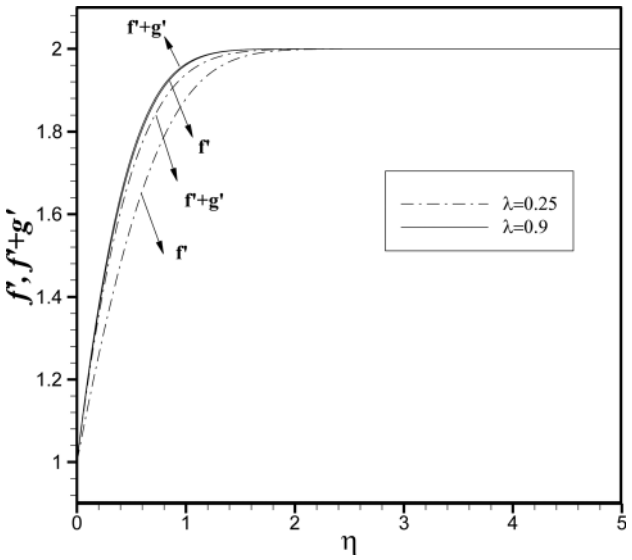

Fig. 9 Effect of the velocity ratio λ on dimensionless velocity profiles f' and $(f'+g')$ when $\gamma = 2.0$ and $\beta = 0.5$

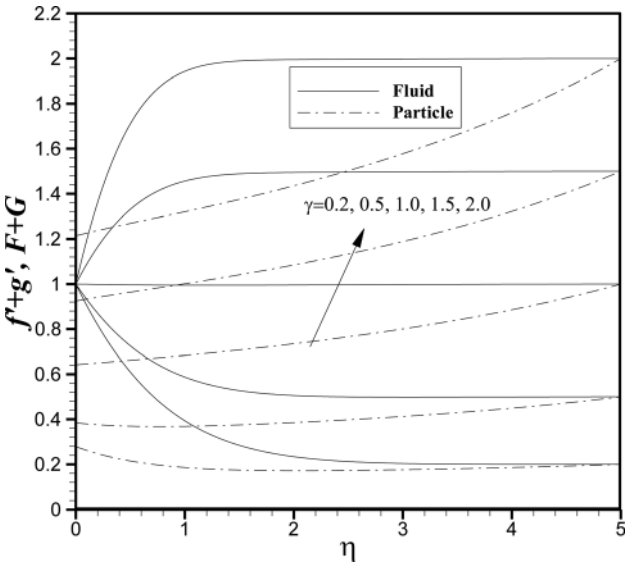

Fig. 11 Dimensionless profiles of v, v_p velocity components for different values of γ when $\lambda = 0.5$ and $\beta = 0.5$

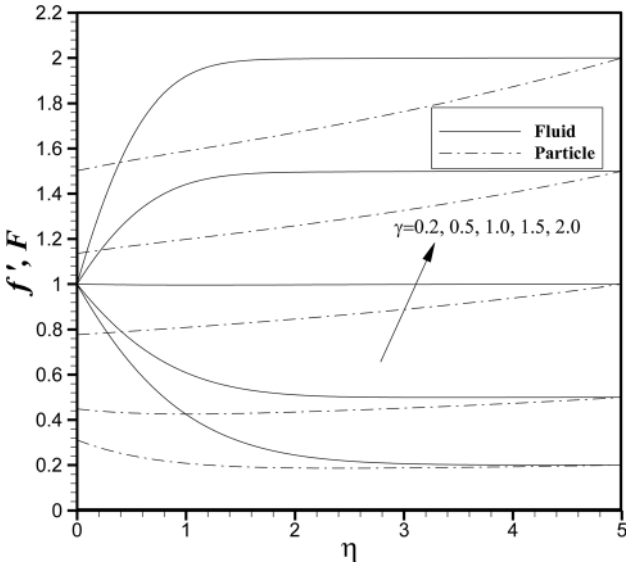

Fig. 10 Dimensionless profiles of u, u_p velocity components for different values of γ when $\lambda = 0.5$ and $\beta = 0.5$

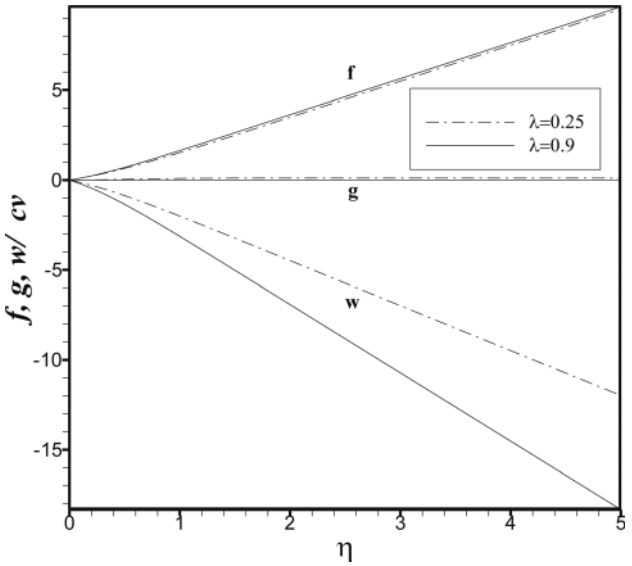

Fig. 12 Effect of velocity ratio λ parameter on f, g, and dimensionless velocity profiles $w/\sqrt{cv}$ when $\gamma = 2.0$ and $\beta = 0.5$

fluid–particle interaction parameter β, the ratio of the freestream velocity parameter to the stretching sheet velocity parameter γ, the thermal fluid–particle interaction parameter β_T, the Prandtl number Pr, and the Eckert number Ec are presented. In order to validate the results presented in this paper, different quantities are selected and compared with those of Refs. [24,26] for the two-dimensional case in Table 1. As it can be seen, an excellent agreement is reported.

In order to verify the accuracy of our present method, and to observe the difference between the 2D and 3D cases, the comparison of the velocity gradient in x direction on the wall, $f''(0)$, with those of the previously published results of Refs. [24,26], for different values of γ was made. The result of this comparison shows an excellent agreement in all the above cases which is a confirmation of the accuracy of our obtained results. Also, comparing the results in the fourth and fifth columns (2D and axisymmetric cases) shows that the shear stress for the axisymmetric case is larger than for the 2D case, as expected, since the thermal and velocity boundary layer in the 2D case is smaller than the axisymmetric case.

Shear stress coefficient in x and y directions and heat transfer on the wall are presented in Table 2 in third, fourth, and fifth columns, respectively, for different values of γ and λ. Comparing the results in the 3D ($\lambda < 1$) and the axisymmetric ($\lambda = 1$)) cases reveals this important point that the shear stress coefficient in both x and y directions and the heat transfer coefficient in the vicinity of the plate increase by increasing λ and these values are the largest for the axisymmetric case ($\lambda = 1$).This can also be observed from Figs. 2–7. Moreover, by comparing the results in rows $\gamma = 0.2$ and $\gamma = 2.0$, one can observe that the sign of the shear stress coefficients is different. This is because when the stretching velocity is less than the freestream velocity ($\gamma > 1$), the flow has a boundary layer structure. On the other hand, when $\gamma < 1$, the flow has an inverted boundary layer structure (Figs. 8 and 9).

In the following, results of the exact solution are illustrated in Figs. 2–33. Figures 10 and 11 illustrate variation of the velocity profiles for different values of γ. Again, it is found that when the

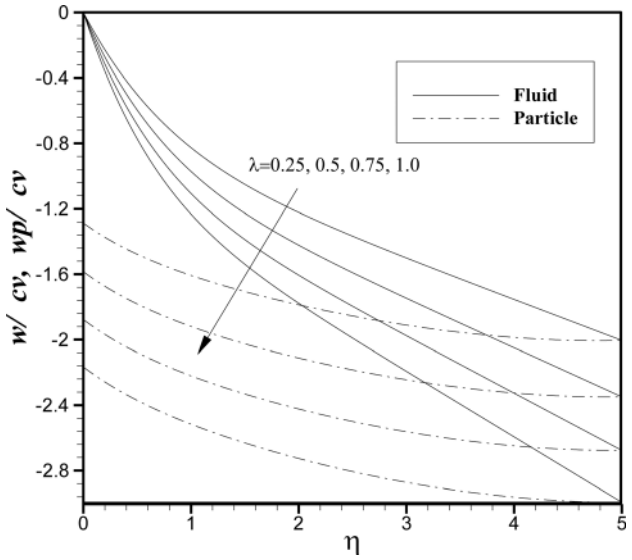

Fig. 13 Dimensionless profiles of w, w_p velocity components for different values of λ when $\gamma = 0.2$ and $\beta = 0.5$

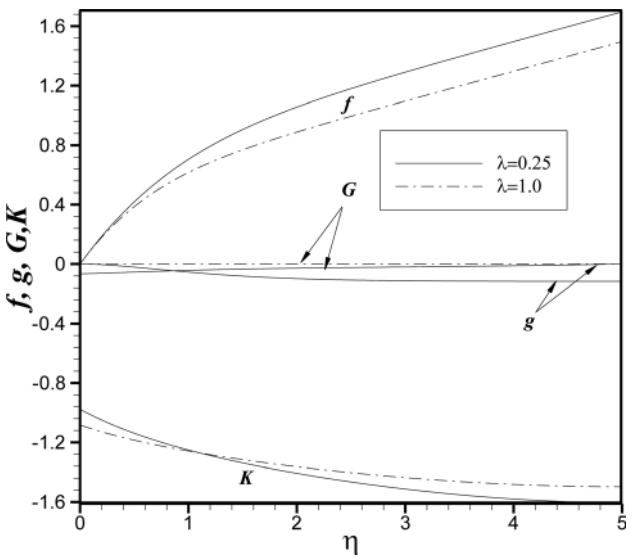

Fig. 14 Dimensionless profiles of f, g, G, and K for different values of λ when $\gamma = 0.2$ and $\beta = 0.5$

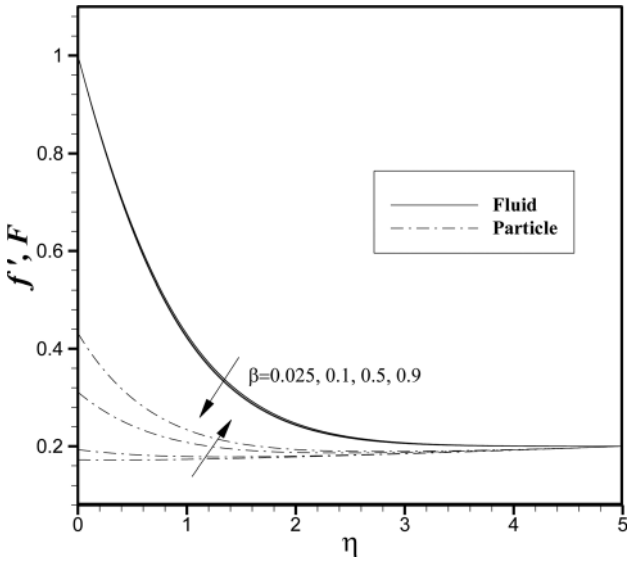

Fig. 15 Dimensionless profiles of u, u_p velocity components for different values of β when $\lambda = 0.5$ and $\gamma = 0.2$

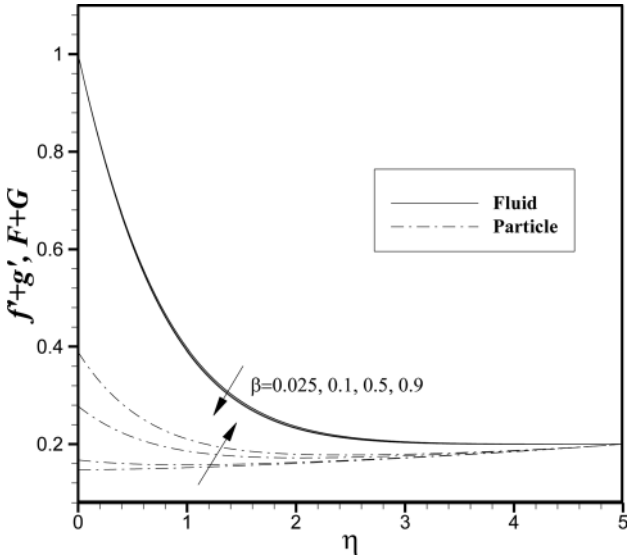

Fig. 16 Dimensionless profiles of v, v_p velocity components for different values of β when $\lambda = 0.5$ and $\gamma = 0.2$

stretching velocity is less than the freestream velocity ($\gamma > 1$), the flow has a boundary layer structure and on the other hand, when $\gamma > 1$, the flow has an inverted boundary layer structure. As it can be seen from Figs. 10 and 11, when $\gamma = 1$, the velocity profiles are straight lines, which means that for this case shear stress ($\lambda f''(0)$ and $f''(0) + g''(0)$) is zero. This is a logical result because the stretching velocity is equal to the freestream velocity, so there is no boundary layer formation. Also, unlike the state $\gamma < 1$ when $\gamma > 1$, the boundary layer thickness decreases with increase in γ (η_∞ is decreased).

The effect of the velocity ratio λ on the profiles of g', $(f', f' + g')$ and (f, g, w) is shown in Figs. 8, 9, and 12. As it is seen in Figs. 8 and 9, the smaller the λ, the bigger g' and therefore the difference between the velocity components is larger. When $\lambda \to 1$, then $g' \to 0$ (Fig. 12) and $g \to 0$ (Fig. 12) and the two velocity components (u, v) become the same, which validates our result compared to the axisymmetric problem case.

The dimensionless velocity profiles proportional to u, v, and w velocity components are depicted in Figs. 2–13, respectively, for different values of λ and for both the clean and dusty fluid and for $\gamma < 1$ (γ=0.2). As it is seen, the behavior of the clean and dusty fluid is the same and decreases with increase in λ. Also, the bigger the λ, the larger is the absolute value of the w component of the velocity, as expected.

The profiles of f, g, G, and K are shown in Fig. 14. As previously was mentioned, since g and G are due to nonaxisymmetric problem, then when $\lambda \to 1$, g and G tend to zero.

Note that, as $\lambda \to 0$, governing equations for the dusty-flow appear in the new forms which are definitely different from the governing equations of the two-dimensional problem case [19–24] because λ tends to zero gradually and the basic governing equations remain three-dimensional. Note that the existence of the physical limitation in the x direction is the cause of the gradual change in λ from one to zero.

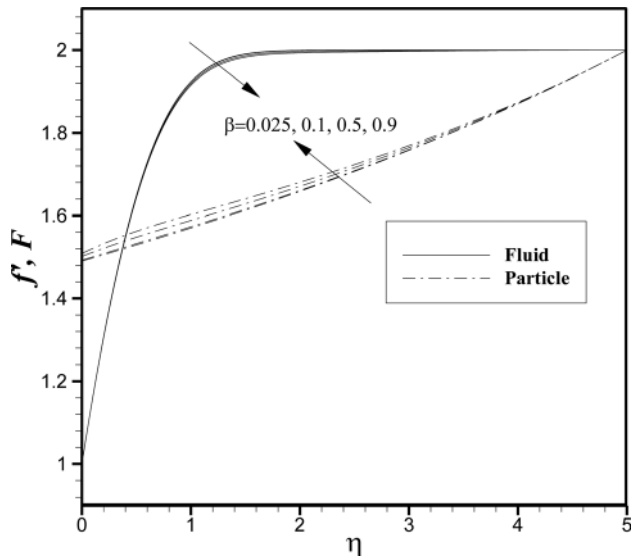

Fig. 17 Dimensionless profiles of u, u_p velocity components for different values of β when $\lambda = 0.5$ and $\gamma = 2.0$

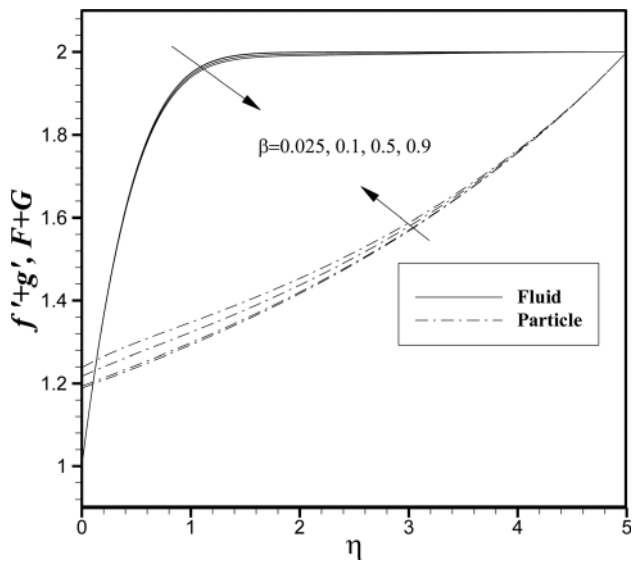

Fig. 18 Dimensionless profiles of v, v_p velocity components for different values of β when $\lambda = 0.5$ and $\gamma = 2.0$

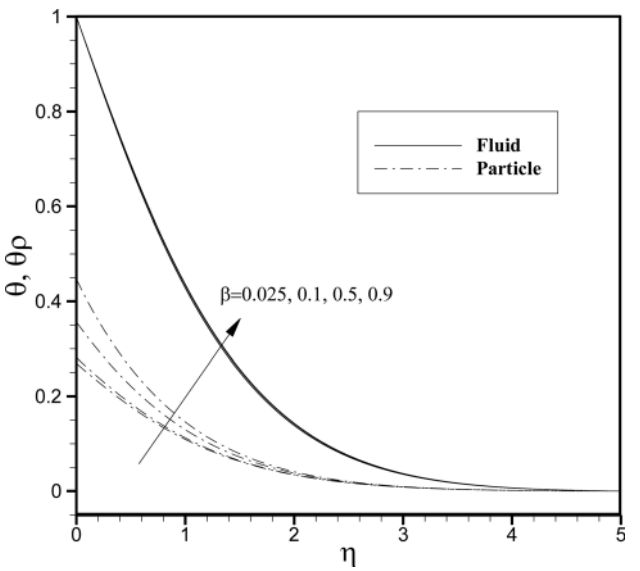

Fig. 19 Dimensionless temperature profiles for different values of β when λ=0.5, $\gamma = 0.2$, Pr = 0.72, and $Ec_x = Ec_y = 1.0$

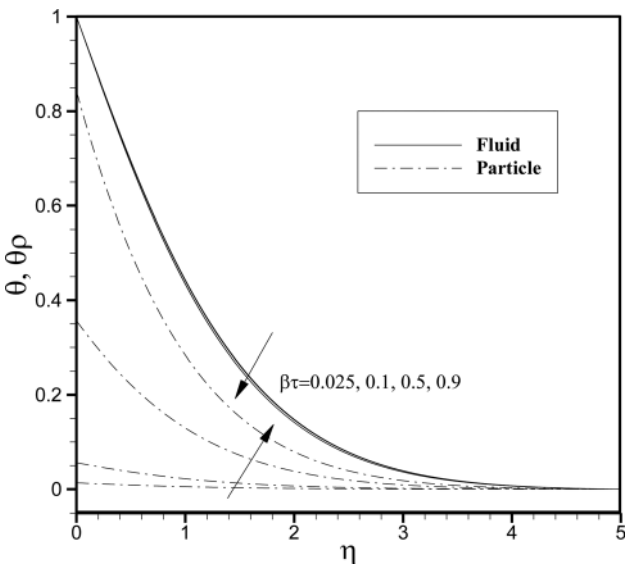

Fig. 20 Dimensionless temperature profiles for different values of β_T when λ=0.5, $\gamma = 0.2$, Pr = 0.72, and $Ec_x = Ec_y = 1.0$

The dimensionless velocity profiles proportional to u and v velocity components, respectively, for different values of λ for both the clean and dusty fluid and for $\gamma > 1$ ($\gamma = 2.0$) are presented in Figs. 4 and 5. For velocity profiles in the x direction (Fig. 4), unlike inverted boundary layer structure $\gamma < 1$ (Fig. 2), the behavior of the clean and the dusty fluid is adverse with increase in λ.The u velocity component of the fluid increases with increase in λ while the u_p velocity component of the dusty fluid decreases (Fig. 4). For velocity profiles in the y direction (Fig. 5), similar to inverted boundary layer structure $\gamma < 1$ (Fig. 3), the behavior of the clean and dusty fluid is the same. But, unlike the case of $\gamma < 1$, the dusty and fluid velocities increase with increase in λ (Fig. 5).

The velocity profile variations in the boundary layer for different values of the fluid–particle interaction parameter β are presented in Figs. 15–18 for $\gamma = 0.2$ and $\gamma = 2.0$, respectively. As it is seen, the values of the velocity are higher for the clean fluid than for the dusty fluid at all points (except for some points near the wall in $\gamma = 2.0$), as expected. Also, it is found that the same effects in the cases of $\gamma < 1$, and $\gamma > 1$ but adverse effect in the clean and dusty flow, as when β increases the clean fluid velocity f' decreases whereas the dusty fluid velocity $F(\eta)$ increases. Of course the effect of the variation of β is more sensible on dusty phase than for the fluid phase since the increase in β increases the contribution of particles of the fluid velocity and so decreases the fluid velocity. This is evident because for the large values of β ($\tau \to 0$), the relaxation velocity time of the dusty fluid decreases and therefore the velocities of both the fluid and dusty phase will be the same. So, by increase in β the velocity profiles of dusty and fluid phases are close to each other.

5.1 Energy Equation Results. The variation of dimensionless temperature profiles θ, θ_p for various values of λ and selected values of β, β_T, Pr, and Ec are presented in two cases of $\gamma < 1$

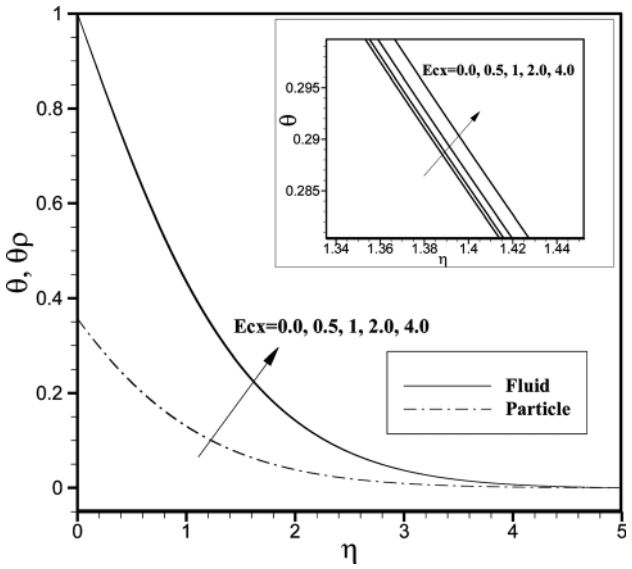

Fig. 21 Dimensionless temperature profiles for different values of Ec_x when $\lambda = 0.5$, $\gamma = 0.2$, $\beta = 0.5$, $\beta_T = 0.5$, and Pr = 0.72

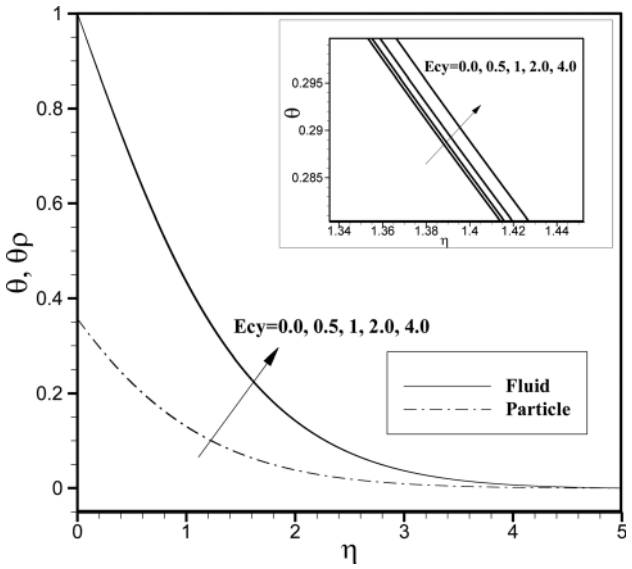

Fig. 22 Dimensionless temperature profiles for different values of Ec_y when $\lambda = 0.5$, $\gamma = 0.2$, $\beta = 0.5$, $\beta_T = 0.5$, and Pr = 0.72

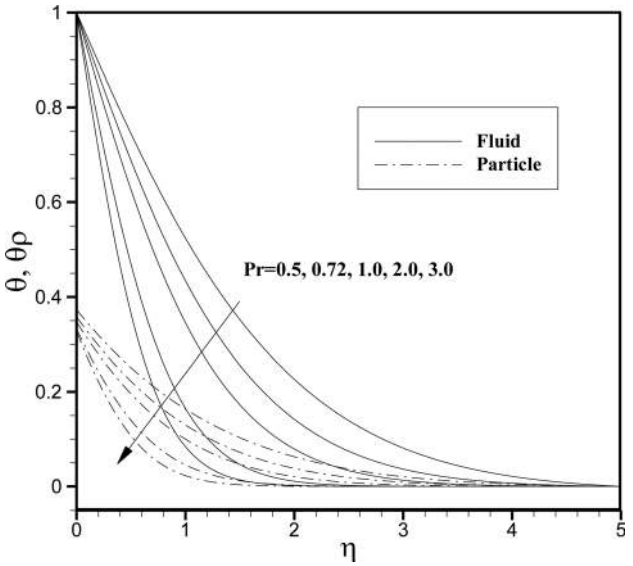

Fig. 23 Dimensionless temperature profiles for different values of Pr when $\lambda = 0.5$, $\gamma = 0.2$, $\beta = 0.5$, $\beta_T = 0.5$, and $Ec_x = Ec_y = 1.0$

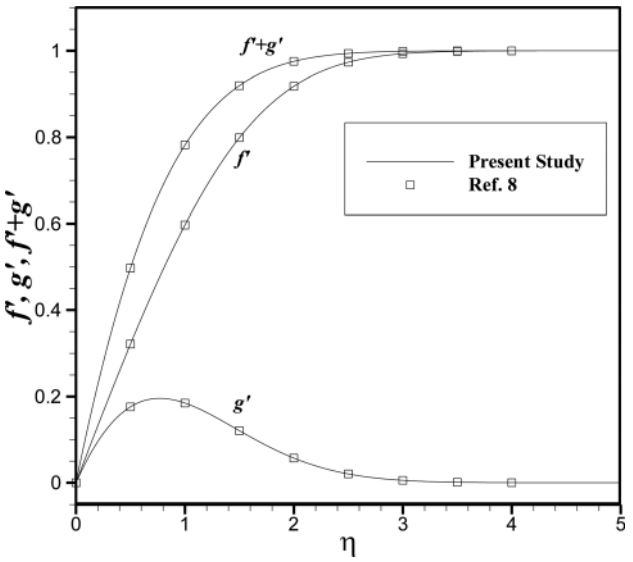

Fig. 24 Comparison of dimensionless velocity profiles f', g', and $f'+g'$ when $\lambda = 0.1$

(Fig. 6) and $\gamma > 1$ (Fig. 7). As it is seen, increase of λ causes decrease of the temperature profile of both the dusty and fluid phases. It is also noted that, for $\lambda \to 0$, the variation of temperature profiles show validation of the nonaxisymmetric temperature compared to the axisymmetric problem case, again. Moreover, it can be found out from this figure that the coefficient of heat transfer $\theta'(0)$ is larger in axisymmetric case than that of the three-dimensional (also according to Table 2). Furthermore, one can observe from these figures that the values of the temperature are higher for the clean fluid than for the dusty fluid at all points, as excepted.

The variation of the temperature profiles for different values of the fluid and thermal particle interaction parameter β and β_T are presented in Figs. 19 and 20, respectively. It can be seen from Fig. 19 that the temperature of both the clean and dusty fluid decreases with increase in β and of course the effect of variation of β is more sensible on dusty phase than for the fluid phase. This is because of the direct effect of β on velocity and since the temperature depends on velocity, then the temperature varies with variation of β. In Fig. 20, an adverse effect is found for the clean and dusty flow, as when β_T increases the clean fluid temperature θ decreases, whereas the dusty fluid temperature θ_p increases. This is similar to the trend of variation of the velocity for different values of β (Figs. 15 and 16). This is because for the large values of β_T ($\tau_T \to 0$), the thermal relaxation temperature time of the dusty fluid decreases and then the temperatures of both the fluid and dusty phases will be the same.

The effect of the Eckert number Ec on the temperature in the boundary layer thickness has been plotted in Figs. 21 and 22. One can observe from these figures that this effect can be neglected. The dissipation term $(u_p - u)F_p$ due to particles moving relative to the fluid is usually very small (here $(F - f') < 1$ so $(F - f')^2 \ll 1$), so productive terms $\mathrm{Ec}_x(F - f')^2$ for Ec_x of order one are still small. So, the variations of the Ec number on

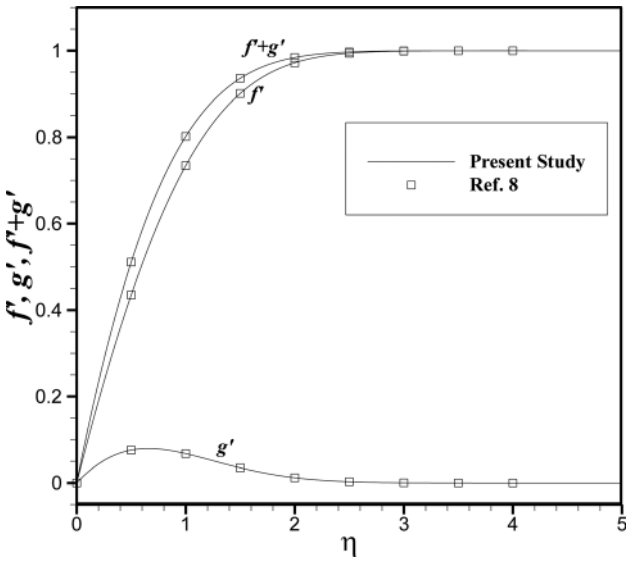

Fig. 25 Comparison of dimensionless velocity profiles f', g', and $f'+g'$ when λ=0.5

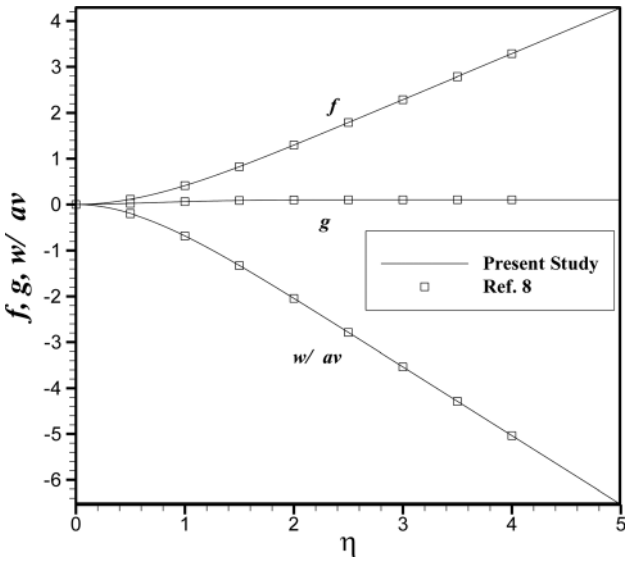

Fig. 27 Comparison of dimensionless profiles f, g and velocity profile $w/\sqrt{av}$ when $\lambda = 0.5$

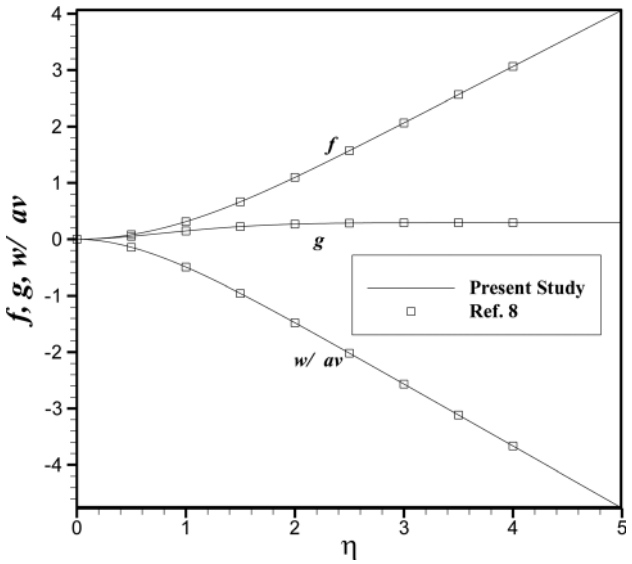

Fig. 26 Comparison of dimensionless profiles f, g and velocity profile $w/\sqrt{av}$ when $\lambda = 0.1$

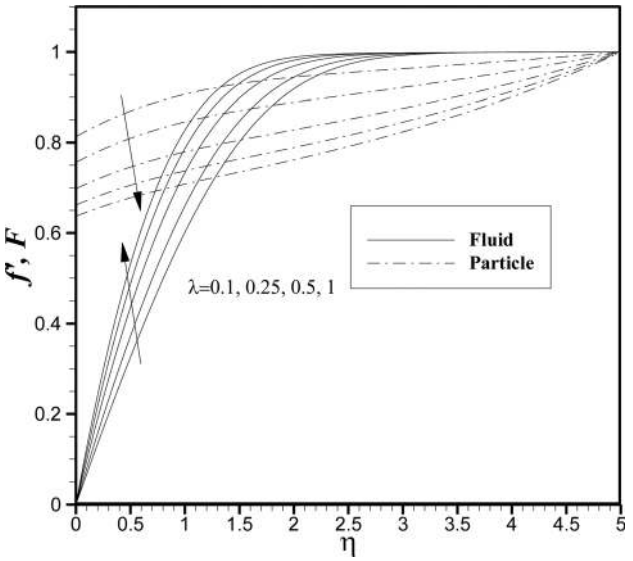

Fig. 28 Dimensionless profiles of u, u_p velocity components for different values of λ when $\beta = 0.5$

temperature profiles are neglected in the area of engineering application of this problem (Ec $= O(1)$ and smaller).

The dimensionless temperature profiles for different values of Prandtl numbers are presented in Fig. 23. As it can be seen, the fluid phase temperature and the dusty phase temperature decrease with increase of Prandtl number. As with the increase of Pr number, the depth of diffusion of the thermal boundary layer decreases and the thermal boundary layer is thinner than the momentum boundary layer; consequently, the temperature gradient increases with the increase in Prandtl number (Table 2).

Hereafter, numerical results for the exact solution of the three-dimensional stagnation-point flow and heat transfer on the stationary plate are presented.

For a pure fluid flow $\beta' = \beta'_T = 0$, validation of the results is presented again using different quantities like profiles of g', $(f', f' + g')$, and $(f, g, w/\sqrt{a\nu})$ and are compared with those of Ref. [9] for the cases of λ=0.1 in Figs. 24 and 26 and $\lambda = 0.5$ in Figs. 25 and 27, which all show excellent agreements.

The dimensionless velocity profiles proportional to u and v components of velocity, respectively, for different values of λ and for both the clean and dusty fluid are depicted in Figs. 28 and 29. As it can be seen, behavior of the dusty and the clean fluid is similar to the behavior of stagnation-point flow on stretching sheet when the stretching velocity is less than the freestream velocity $\gamma > 1$ (flow has boundary layer structure).

The velocity and temperature profiles variations in boundary layer for different values of fluid particle interaction parameter β' and β'_T, respectively, are presented in Figs. 30–33. As it is seen, the trend of these variations is similar to the case of stretching sheet results. It means that when β' increases the clean fluid velocity decreases, whereas the dusty fluid velocity increases. Also, when β'_T increases the clean fluid temperature decreases, whereas the dusty fluid temperature increases.

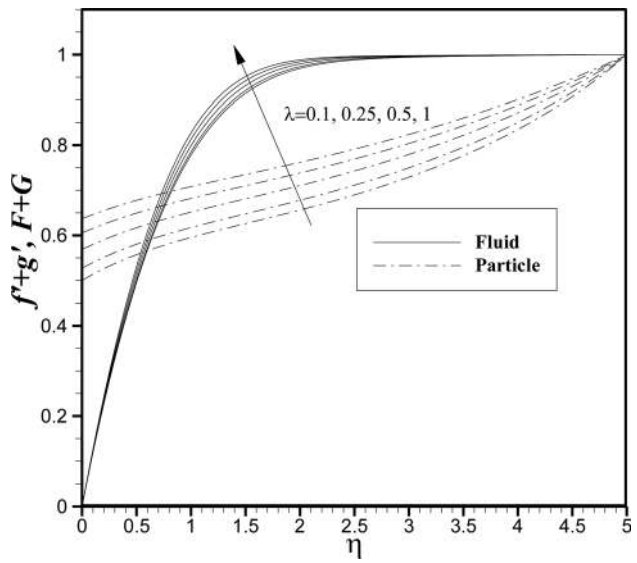

Fig. 29 Dimensionless profiles of v, v_p velocity components for different values of λ when $\beta = 0.5$

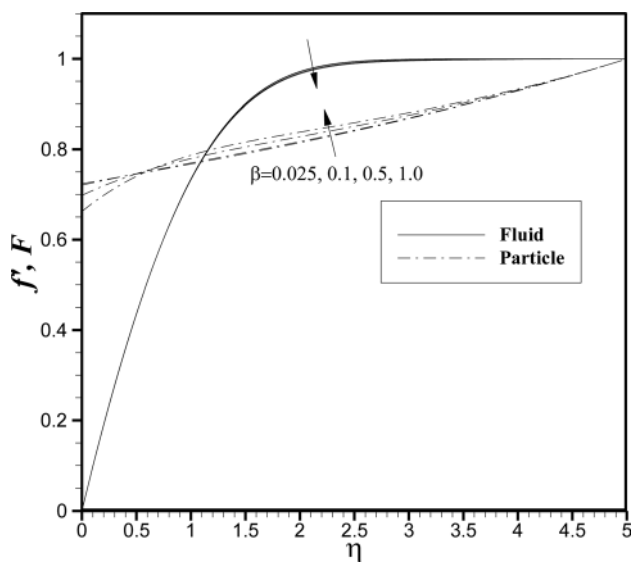

Fig. 30 Dimensionless profiles of u, u_p velocity components for different values of β when $\lambda = 0.5$ and $\gamma = 0.2$

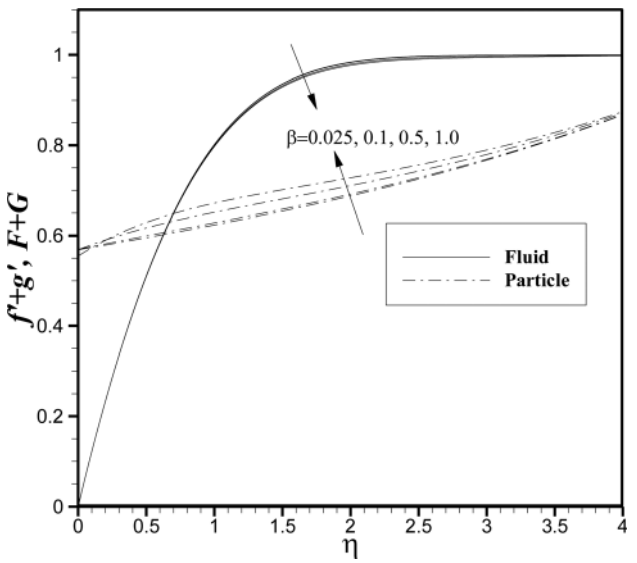

Fig. 31 Dimensionless profiles of v, v_p velocity components for different values of β when $\lambda = 0.5$ and $\gamma = 0.2$

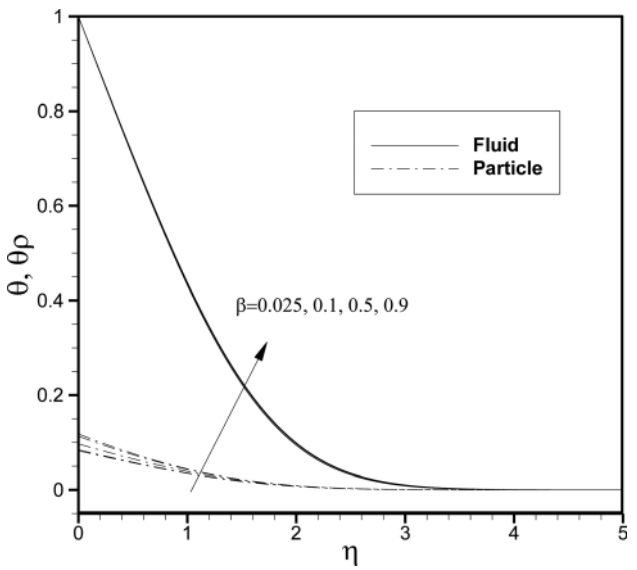

Fig. 32 Dimensionless temperature profiles for different values of β when $\lambda = 0.5$ and $\gamma = 0.2$

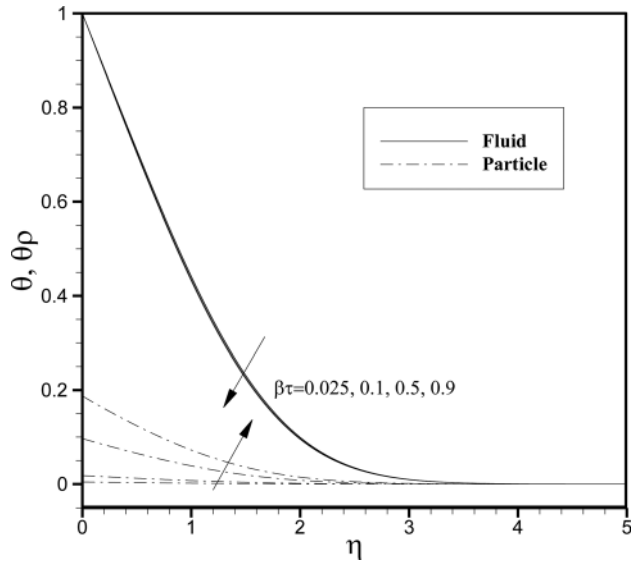

Fig. 33 Dimensionless temperature profiles for different values of β_T when $\lambda = 0.5$ and $\gamma = 0.2$

6 Conclusions

In the present study, the effects of different parameters on the velocity profiles and temperature profiles of a dusty fluid over a stretching sheet and a stationary flat plate have been investigated and illustrated for both dusty and fluid phases. An exact solution for axisymmetric and nonaxisymmetric three-dimensional case of problem have been presented via converting governing partial differential equations into ordinary differential equations by appropriate similarity transformations. Since the three-dimensional case of this problem is closer to reality and practical purposes, we are interested to model it and to know what happens and how components of the flow vary when effect of the third dimension is considered. For this reason, the effects of the third dimension in axisymmetric ($\lambda = 1$) and nonaxisymmetric ($\lambda \neq 1$) cases have been investigated. Also, the effects of the physical parameters on the velocity and the temperature fields and the dusty phase have been shown graphically and discussed where no attempts had been made to analyze this problem previously. It has been found that increasing velocity ratio λ causes the value of the fluid velocity components in x and y directions to decrease, for $\gamma < 1$ case, and to increase for $\gamma > 1$. Also, it has been shown that increasing the velocity ratio λ causes the value of the temperature in boundary layer to decrease, for both cases of $\gamma < 1$ and $\gamma > 1$. So, the velocity and temperature gradients increase by increase in λ. For $\lambda = 1$, the axisymmetric case, these gradients are maximum. As a result, the shear stress and heat transfer on the wall increase with increase in λ. It is very interesting to note that the effect of β is adverse in clean and dusty flow in both cases of $\gamma < 1$ and $\gamma > 1$, as when β increases the clean fluid velocity decreases whereas the dusty fluid velocity increases. Of course it has been deduced that the effect of variation of β is more sensible on dusty phase than on the fluid phase. Similarly, one can observe the same effects on clean and dusty flow temperature profiles because of β_T. Moreover, one can observe that there is no significant change in the temperature profiles since the order of dissipation work term in energy equation is very small. Also for the stationary flat plate case, a similarity solution has been presented. The results show the same behavior in velocity and temperature profiles for both the dusty and fluid phases with stretching sheet case for $\gamma > 1$ (boundary layer structure) in general since in both the flat plate and stretching sheet cases for $\gamma > 1$, freestream velocity is larger than the wall velocity. The numerical results give a view toward understanding the response characteristics of the dusty fluid as two-phase flow. This study can be a base model for combustion in a stagnation-flow problem where the fluid phase changes into vaporized bubbles upon impact on a heated substrate and thereafter could go through the process of combustion if ignition takes place.

References

[1] Sakiadis, B. C., 1961, "Boundary Layer Behavior on Continuous Solid Surface," AIChE J., **7**(1), pp. 26–28.
[2] Crane, L. J., 1970, "Flow Past a Stretching Sheet," Z. Angew. Math. Phys., **21**(4), pp. 645–647.
[3] Hiemenz, K., 1911, "Die grenzchicht an einem in den gleichformingen Flussigkeitsstrom eingetauchten geraden KreisZylinder," Dinglers Polytech. J., **326**, pp. 321–410.
[4] Homman, F. Z., 1936, "Der Einfluss Grosser Zahighkeit bei der Strmung um den Zylinder und um die Kugel," Z. Angew. Math. Mech., **16**(3), pp. 153–164.
[5] Chiam, T. C., 1994, "Stagnation-Point Flow Towards a Stretching Plate," J. Phys. Soc. Jpn., **63**(6), pp. 2443–2444.
[6] Ishak, A., Jafar, K., Nazar, R., and Pop, I., 2009, "MHD Stagnation Point Flow Towards a Stretching Sheet," Phys. A, **388**(17), pp. 3377–3383.
[7] Ishak, A., Nazar, R., and Pop, I., 2008, "Hydromagnetic Flow and Heat Transfer Adjacent to a Stretching Vertical Sheet," Heat Mass Transfer, **44**(8), pp. 921–927.
[8] Tzirtzilakis, E. E., and Kafoussias, N. G., 2009, "Three-Dimensional Magnetic Fluid Boundary Layer Flow Over a Linearly Stretching Sheet," ASME J. Heat Transfer, **132**(1), p. 011702.
[9] Abbassi, A. S., and Rahimi, A. B., 2009, "Non-Axisymmetric Three-Dimensional Stagnation-Point Flow and Heat Transfer on a Flat Plate," ASME J. Fluids Eng., **131**(7), p. 074501.
[10] Abbassi, A. S., and Rahimi, A. B., 2009, "Three-Dimensional Stagnation Flow and Heat Transfer on a Flat Plate With Transpiration," J. Thermophys. Heat Transfer, **23**(3), pp. 513–521.
[11] Abbassi, A. S., Rahimi, A. B., and Niazman, H., 2011, "Exact Solution of Three-Dimensional Unsteady Stagnation Flow on a Heated Plate," J. Thermophys. Heat Transfer, **25**(1), pp. 55–58.
[12] Abbassi, A. S., and Rahimi, A. B., 2012, "Investigation of Two-Dimensional Unsteady Stagnation-Point Flow and Heat Transfer Impinging on an Accelerated Flat Plate," ASME J. Heat Transfer, **134**(6), p. 064501.
[13] Kuznetsov, A. V., and Nield, D. A., 2010, "Natural Convective Boundary-Layer Flow of a Nanofluid Past a Vertical Plate," Int. J. Therm. Sci., **49**(2), pp. 243–247.
[14] Kuznetsov, A. V., and Nield, D. A., 2011, "Double-Diffusive Natural Convective Boundary-Layer Flow of a Nanofluid Past a Vertical Plate," Int. J. Therm. Sci., **50**(5), pp. 712–717.
[15] Mustafa, M., Hayat, T., Pop, I., Asghar, S., and Obaidat, S., 2011, "Stagnation-Point Flow of a Nanofluid Towards a Stretching Sheet," Int. J. Heat Mass Transfer, **54**(25–26), pp. 5588–5594.
[16] Makinde, O. D., Khan, W. A., and Khan, Z. H., 2013, "Buoyancy Effects on MHD Stagnation Point Flow and Heat Transfer of a Nanofluid Past a Convectively Heated Stretching/Shrinking Sheet," Int. J. Heat Mass Transfer, **62**, pp. 526–533.
[17] Mahapatra, T. R., Samir, K. N., and Pop, I., 2014, "Dual Solutions in Stagnation-Point Flow and Heat Transfer Over a Shrinking Surface With Partial Slip," ASME J. Heat Transfer, **136**(10), p. 104501.
[18] Sinha, A., and Misra, J. C., 2014, "Effect of Induced Magnetic Field on Magneto-Hydrodynamic Stagnation Point Flow and Heat Transfer on a Stretching Sheet," ASME J. Heat Transfer, **136**(11), p. 112701.
[19] Saffman, P. G., 1962, "On the Stability of Laminar Flow of a Dusty Gas," J. Fluid Mech., **13**(01), pp. 120–128.
[20] Marble, F. E., 1970, "Dynamics of Dusty Gases," Annu. Rev. Fluid Mech., **2**(1), pp. 397–446.
[21] Chakrabarti, K. M., 1974, "Note on Boundary Layer in a Dusty Gas," AIAA J., **12**(8), pp. 1136–1137.
[22] Datta, N., and Mishra, S. K., 1982, "Boundary Layer Flow of a Dusty Fluid Over a Semi-Infinite Flat Plate," Acta Mech., **42**(1), pp. 71–83.
[23] Vajravelu, K., and Nayfeh, J., 1992, "Hydro-Magnetic Flow of a Dusty Fluid Over a Stretching Sheet," Int. J. Non-Linear Mech., **27**(6), pp. 937–945.
[24] Gireesha, B. J., Roopa, G. S., and Bagewadi, C. S., 2012, "Effect of Viscous Dissipation and Heat Source on Flow and Heat Transfer of Dusty Fluid Over Unsteady Stretching Sheet," Appl. Math. Mech., **33**(8), pp. 1001–1014.
[25] Gireesha, B. J., Ramesh, G. K., Abel, M. S., and Bagewadi, C. S., 2011, "Boundary Layer Flow and Heat Transfer of a Dusty Fluid Flow Over a Stretching Sheet With Non-Uniform Heat Source/Sink," Int. J. Multiphase Flow, **37**(8), pp. 977–982.
[26] Ramesh, G. K., and Gireesha, B. J., 2013, "Flow Over a Stretching Sheet in a Dusty Fluid With Radiation Effect," ASME J. Heat Transfer, **135**(10), p. 102702.
[27] Ramesh, G. K., Gireesha, B. J., and Bagewadi, C. S., 2012, "MHD Flow of a Dusty Fluid Near the Stagnation Point Over a Permeable Stretching Sheet With Non-Uniform Source/Sink," Int. J. Heat Mass Transfer, **55**(17–18), pp. 4900–4907.
[28] Ramesh, G. K., Gireesha, B. J., and Bagewadi, C. S., 2014, "Stagnation Point Flow of a MHD Dusty Fluid Towards a Stretching Sheet With Radiation," Afr. Mat., **25**(1), pp. 237–249.
[29] Ismail, A. M., and Ganesh, S., 2014, "Exact Solution to Unsteady MHD Dusty Fluid Flow Over a Moving Horizontal Plate Through a Porous Space," Paripex—Indian J. Res., **3**(2), pp. 204–207.
[30] Singh, P., Jangid, A., Tomer, N. S., and Sinha, D., 2010, "Effects of Thermal Radiation and Magnetic Field on Unsteady Stretching Permeable Sheet in Presence of Free Stream Velocity," Int. J. Inf. Math. Sci., **3**, pp. 160–166.